An enhanced finite element algorithm for thermal Darcy flows with variable viscosity

Loubna Salhi[1], Mofdi El-Amrani[2], and Mohammed Seaid[3,4]

[1] Laboratory Modeling Simulation & Data Analysis, University Mohammed VI Polytechnic, Benguerir, Morocco
[2] Mathematics and Applications Laboratory, FST, Abdelmalek Essaadi University, Tangier, Morocco
[3] Department of Engineering, University of Durham, South Road, Durham DH1 3LE, UK
[4] International Water Research Institute, University Mohammed VI Polytechnic, Benguerir, Morocco

Abstract. This paper deals with the development of a stable and efficient unified finite element method for the numerical solution of thermal Darcy flows with variable viscosity. The governing equations consist of coupling the Darcy equations for the pressure and velocity fields to a convection-diffusion equation for the heat transfer. The viscosity in the Darcy flows is assumed to be nonlinear depending on the temperature of the medium. The proposed method is based on combining a semi-Lagrangian scheme with a Galerkin finite element discretization of the governing equations along with an robust iterative solver for the associate linear systems. The main features of the enhanced finite element algorithm are that the same finite element space is used for all solutions to the problem including the pressure, velocity and temperature. In addition, the convection terms are accurately dealt with using the semi-Lagrangian scheme and the standard Courant-Friedrichs-Lewy condition is relaxed and the time truncation errors are reduced in the diffusion terms. Numerical results are presented for two examples to demonstrate the performance of the proposed finite element algorithm.

Keywords: Thermal Darcy flows · Unified finite elements · Semi-Lagrangian method · Moving fronts.

1 Introduction

In the present study, given a bounded two-dimensional domain $\Omega \subset \mathbb{R}^2$ with Lipschitz continuous boundary Γ and a time interval $[0, T]$, we focus on solving a time-dependent heat equation coupled with the Darcy equations. For all $(\mathbf{x}, t)$ in the domain $\Omega \times [0, T]$, the governing equations read

$$\begin{aligned} \nu(\Theta)\boldsymbol{u} + \nabla p &= \boldsymbol{f}(\Theta), && \text{in} \quad \Omega, \\ \nabla \cdot \boldsymbol{u} &= 0, && \text{in} \quad \Omega, \end{aligned} \tag{1a}$$

$$\frac{D\Theta}{Dt} - \kappa \nabla^2 \Theta = g(\boldsymbol{x}, t), \qquad \text{in} \quad \Omega, \tag{1b}$$

ICCS Camera Ready Version 2021
To cite this paper please use the final published version:
DOI: 10.1007/978-3-030-77980-1_17

where $\boldsymbol{u}$ is the velocity field, p the pressure and Θ the fluid temperature. In the Darcy equations (1a), ν is the variable viscosity and $\boldsymbol{f}$ the force density which both are dependent on the temperature. In the heat equation (1b), κ is the thermal diffusivity coefficient supposed to be a positive constant, g an external source term and

$$\frac{D\Theta}{Dt} = \frac{\partial \Theta}{\partial t} + \boldsymbol{u} \cdot \nabla \Theta, \tag{1c}$$

is the total derivative which measures the temperature rate of change along the trajectories of the fluid particles known by characteristic curves. The system of equations (1a)-(1b) is equipped with an initial condition

$$\Theta(\boldsymbol{x}, 0) = \Theta_0(\boldsymbol{x}), \qquad \text{in} \quad \Omega, \tag{1d}$$

as well as given boundary conditions. In view of simplification, homogeneous Dirichlet boundary conditions are considered for the pressure and temperature, while a no-slip boundary condition is prescribed on the velocity:

$$p = 0 \quad \text{and} \quad \boldsymbol{u} \cdot \boldsymbol{n} = 0, \qquad \text{on} \quad \Gamma, \tag{1e}$$

$$\Theta = 0, \qquad \text{on} \quad \Gamma, \tag{1f}$$

where $\boldsymbol{n}$ is the unit outward normal vector on the boundary Γ. Notice that the present study easily extends to different types of boundary conditions without major conceptual changes in the formulation. It should be stressed that the system of equations (1) has been widely used in the literature to model several applications of fluid mechanics such as transport of contaminants in saturated zones and aquifers, heat explosion problems in the chemical industry, nuclear waste and carbon dioxide geological storage, see [2,10,11,20,26,27] among others. In bio-medical fields, the model has also been used to study the so-called bio-heat transfer, the arterial and venous blood flows by considering the human body as a deformable porous medium, see for instance [21,22,30]. While the mathematical theory and existence of a weak solution for the problem (1) is well developed in the literature [9,17], the numerical resolution is still challenging for several reasons. Especially, when the diffusion term is negligible in comparison with the convective term. In such a case, the numerical solution give rise to serious computational difficulties by generating either non-physical oscillations or numerical dissipation in the presence of steep fronts and shocks, see for instance [12,13,24,28].

Numerical techniques used to deal with these difficulties include Eulerian finite element methods which are usually easy to implement. However, most Eulerian methods use fixed grids and incorporate some upstream weighting in their formulations to stabilize spatial discretization. In addition, time truncation errors dominate their solutions and are subject to the Courant-Friedrichs-Lewy (CFL) stability conditions, which impose a sever restriction on the size of the time steps taken in numerical simulations. In the current work, we use a semi-Lagrangian finite element method to deal with the transport equation in (1). This class of methods has been used for solving many convection-dominated

ICCS Camera Ready Version 2021
To cite this paper please use the final published version:
DOI: 10.1007/978-3-030-77980-1_17

flow problems, see for example [12,13,23,24,27,26]. The main advantage in these methods is that they allow to convert the temperature equation in (1) from an Eulerian description to a semi-Lagrangian one in terms of the particle trajectories, also known as characteristics, and to treat the transport part (1c) separately in the finite element discretization. Thus, the time derivative and the convection terms are combined as a directional derivative along the particles trajectories, leading to a characteristic time-stepping procedure. This results in a substantial reduction in the computational cost and in the time truncation errors. Moreover, the semi-Lagrangian scheme offers the possibility of using time steps that exceed those allowed by the stability CFL condition for the conventional Eulerian methods, see [14,15,16,26] for further details. Next, to improve the accuracy of the enhanced method, we use a stabilization technique proposed by [5] for spatial discretization of Darcy equations. The main advantage of this technique is that it allows the use of equal-order finite element approximations for all solutions in the problem and thus, it does not require the use of mixed formulations such as those widely employed in the literature, see for instance [1,25]. In [5], it was shown that the stabilization method is unconditionally stable and it allows to achieve optimal accuracy with respect to solution regularity.

This paper is organized as follows. Formulation of the proposed semi-Lagrangian finite element method is presented in section 2. Section 3 is devoted to numerical results for two test examples for coupled Darcy-heat problems. Concluding remarks are presented in Section 4.

2 Semi-Lagrangian finite element method

Let $\Omega_h \subset \bar{\Omega} = \Omega \cup \Gamma$ denotes a quasi-uniform partition of Ω into triangular finite elements $\mathcal{K}_j$ with the partition step h. We define the conforming finite element space for the temperature and pressure as

$$V_h = \Big\{ v_h \in C^0(\Omega) : \quad v_h\big|_{\mathcal{K}_j} \in P_k(\mathcal{K}_j), \quad \forall\, \mathcal{K}_j \in \Omega_h \Big\},$$

where $P_k(\mathcal{K}_j)$ is the space of complete polynomials of degree k, $k \geq 2$, on each element $\mathcal{K}_j$. We also define the conforming finite element space $\mathbf{V}_h = (V_h)^2$ for the velocity field. For time discretization, we divide the time interval $[0, t_N]$ into N equal subintervals $[t_n, t_{n+1}]$ with length $\Delta t = t_{n+1} - t_n$ for $n = 0, 1, \ldots, N$. Then, we formulate the finite element solutions to $\boldsymbol{u}^n(\boldsymbol{x})$, $p^n(\boldsymbol{x})$ and $\Theta^n(\boldsymbol{x})$ as

$$\boldsymbol{u}_h^n(\boldsymbol{x}) = \sum_{j=1}^{M} U_j^n \circ \varphi_j(\boldsymbol{x}), \quad p_h^n(\boldsymbol{x}) = \sum_{j=1}^{M} P_j^n \phi_j(\boldsymbol{x}), \quad \Theta_h^n(\boldsymbol{x}) = \sum_{j=1}^{M} \mathcal{T}_j^n \phi_j(\boldsymbol{x}), \quad (2)$$

were the symbol $\circ$ denotes the hadamard product that produces vectors through element-by-element multiplication of the original two vectors. In (2), U_j^n, P_j^n and $\mathcal{T}_j^n$ are the corresponding nodal values of $\boldsymbol{u}_h^n(\boldsymbol{x})$, $p_h^n(\boldsymbol{x})$ and $\Theta_h^n(\boldsymbol{x})$ respectively defined by $U_j^n = \boldsymbol{u}_h^n(\boldsymbol{x}_j)$, $P_j^n = p_h^n(\boldsymbol{x}_j)$ and $\mathcal{T}_j^n = \Theta_h^n(\boldsymbol{x}_j)$, with $\{\boldsymbol{x}_j\}_{j=1}^M$ being the set of mesh points in the partition Ω_h, $\{\varphi_j\}_{j=1}^M = \{(\phi_j, \phi_j)\}_{j=1}^M$ and $\{\phi_j\}_{j=1}^M$ are the basis vectors and functions of $\mathbf{V}_h$ and V_h respectively given by the Kronecker delta symbol.

ICCS Camera Ready Version 2021
To cite this paper please use the final published version:
DOI: 10.1007/978-3-030-77980-1_17

Next, we define the functional spaces that are useful for the existence and uniqueness of the solution of problem (1). We introduce the Hilbert space

$$H_0^1(\Omega) = \left\{ v \in H^1(\Omega) : \quad v|_\Gamma = 0 \right\}.$$

We also define the space $L_0^2(\Omega)$ of all square integrable functions with vanishing mean as

$$L_0^2(\Omega) = \left\{ w : \ \Omega \longrightarrow \mathbb{R} : \qquad \int_\Omega w d\Omega = 0 \right\}.$$

We define the following inner product and norm in $L^2(\Omega)$:

$$(w, v) = \int_\Omega wv \, d\Omega \qquad \text{and} \qquad \|v\|_{L^2(\Omega)} = (v, v)^{\frac{1}{2}}, \qquad \forall \, w, v \in L^2(\Omega).$$

We recall the standard space:

$$\mathbf{H}_0\left(div, \Omega\right) = \left\{ \mathbf{v} \in \mathbf{H}(div, \Omega) : \quad (\mathbf{v} \cdot \boldsymbol{n})\Big|_\Gamma = 0 \right\}.$$

To approximate the velocity and pressure solutions of the Darcy equations (1a), we shall need the equal-order finite element pair $(\mathbf{S}_h, Q_h)$ defined as

$$\mathbf{S}_h = \mathbf{V}_h \cap \mathbf{H}_0\left(div, \Omega\right) \qquad \text{and} \qquad Q_h = V_h \cap L_0^2(\Omega). \tag{3}$$

We also introduce the necessary finite element space R_h to approximate the temperature solution of the heat equation (1b) as

$$R_h = V_h \cap H_0^1\left(\Omega\right). \tag{4}$$

Notice that the spaces introduced above are necessary to prove the existence and uniqueness of the solution of problem (1), see for instance [4,5,26].

2.1 Solution of the Darcy-heat problem

As in most finite element methods, we start with the weak formulation that reads as : Find $(\boldsymbol{u}, p, \Theta)$ in $\mathbf{H}_0\left(div, \Omega\right) \times L_0^2(\Omega) \times H_0^1(\Omega)$ such that

$$\begin{aligned} \int_\Omega \nu(\Theta)\boldsymbol{u} \cdot \mathbf{s} \, d\Omega - \int_\Omega p \nabla \cdot \mathbf{s} \, d\Omega &= \int_\Omega \boldsymbol{f}(\Theta) \cdot \mathbf{s} \, d\Omega, \qquad && \forall \, \mathbf{s} \in \mathbf{H}_0(div, \Omega), \\ \int_\Omega q \, \nabla \cdot \boldsymbol{u} \, d\Omega &= 0, && \forall \, q \in L_0^2(\Omega), \end{aligned} \tag{5a}$$

$$\int_\Omega \frac{D\Theta}{Dt} r \, d\Omega + \kappa \int_\Omega \nabla\Theta \cdot \nabla r \, d\Omega = \int_\Omega g r \, d\Omega, \qquad \forall \, r \in H_0^1(\Omega). \tag{5b}$$

Note that it is evident to prove that any triplet $(\boldsymbol{u}, p, \Theta)$ in $\mathbf{H}_0(div, \Omega) \times L_0^2(\Omega) \times H_0^1(\Omega)$ solving the problem (1) in the sense of distributions in Ω is a solution of the weak problem (5), see [8,26] for more details. To approximate the velocity, pressure and temperature solutions of system (5a), we use the equal-order finite element spaces $\mathbf{S}_h$, Q_h and R_h defined in (3) and (4), respectively. Note that equations (5a) can also be rewritten as

$$\begin{aligned} \mathcal{A}\left(\boldsymbol{u}_h, \mathbf{s}_h\right) - \mathcal{B}\left(p_h, \mathbf{s}_h\right) &= \mathcal{L}_{\boldsymbol{f}}\left(\mathbf{s}_h\right), \qquad && \forall \, \mathbf{s}_h \in \mathbf{S}_h, \\ \mathcal{B}\left(q_h, \boldsymbol{u}_h\right) &= 0, && \forall \, q_h \in Q_h, \end{aligned} \tag{6}$$

ICCS Camera Ready Version 2021
To cite this paper please use the final published version:
DOI: 10.1007/978-3-030-77980-1_17

where $\mathcal{A}$, $\mathcal{B}$ are the bilinear forms and $\mathcal{L}_{\boldsymbol{f}}$ is the linear form defined as

$$\mathcal{A}(\boldsymbol{u}_h, \mathbf{s}_h) = \int_\Omega \nu(\Theta)\boldsymbol{u}_h \cdot \mathbf{s}_h \, d\Omega, \quad \mathcal{B}(p_h, \mathbf{s}_h) = \int_\Omega p_h \nabla \cdot \mathbf{s}_h \, d\Omega,$$
$$\mathcal{L}_{\boldsymbol{f}}(\mathbf{s}_h) = \int_\Omega \boldsymbol{f}(\Theta_h) \cdot \mathbf{s}_h \, d\Omega.$$

It should also be noted that stable and accurate solutions of the discrete problem (6) are obtained for discrete spaces $\mathbf{S}_h$ and Q_h satisfying the known discrete inf-sup condition [7]. However, the velocity-pressure space $(\mathbf{S}_h, Q_h)$ does not verify the inf-sup condition associated with the mixed form (6), see [5,6,19] for further details. Then, the discrete weak problem is not stable, which makes it necessary to opt for a stabilization technique. To deal with it, we use a polynomial pressure-projection stabilization method which makes that the pair $(\mathbf{S}_h, Q_h)$ verifies a stabilized form of the inf-sup condition [4,5]. Thus, the stabilized weak form of equations (5a) reads as : Find $(\boldsymbol{u}_h, p_h) \in \mathbf{S}_h \times Q_h$ such that

$$\begin{aligned} \mathcal{A}(\boldsymbol{u}_h, \mathbf{s}_h) - \mathcal{B}(p_h, \mathbf{s}_h) &= \mathcal{L}_{\boldsymbol{f}}(\mathbf{s}_h), \qquad \forall\, \mathbf{s}_h \in \mathbf{S}_h, \\ \mathcal{B}(q_h, \boldsymbol{u}_h) &= \mathcal{D}(p_h, q_h), \qquad \forall\, q_h \in Q_h, \end{aligned} \tag{7}$$

where $\mathcal{D}$ is the bilinear form defined as

$$\mathcal{D}(p_h, q_h) = \int_\Omega (p_h - \Pi_{k-1} p_h)(q_h - \Pi_{k-1} q_h) \, d\Omega.$$

Here, Π_{k-1} is the projection operator $\Pi_{k-1} : L^2(\Omega) \longrightarrow [P]_{k-1}$ defined as

$$\Pi_{k-1}(p) = \arg\min \frac{1}{2} \int_\Omega (\Pi_{k-1} q - p)^2 \, d\Omega, \quad \forall q \in [P]_{k-1}, \tag{8}$$

with $[P]_{k-1}$ being the discontinuous polynomial space:

$$[P]_{k-1} = \left\{ q \in L^2(\Omega) : \quad q\Big|_{\mathcal{K}_j} \in P_{k-1}(\mathcal{K}_j), \quad \forall\, \mathcal{K}_j \in \Omega_h \right\}.$$

Next, we use the modified method of characteristics to solve the heat equation (5b). The main idea is to treat the transport term (1c) of equation (5b) in Lagrangian, and separately in the finite element discretization. Then, the new temperature solution is approximated at each time subinterval $[t_n, t_{n+1}]$ using the characteristic curves, also known as the departure points, associated with the material derivative (1c). These characteristic curves are the solutions of the ordinary differential equations

$$\begin{aligned} \frac{d\boldsymbol{X}(\boldsymbol{x}, t_{n+1}; t)}{dt} &= \boldsymbol{u}(\boldsymbol{X}(\boldsymbol{x}, t_{n+1}; t), t), \qquad \forall\, (t, \boldsymbol{x}) \in [t_n, t_{n+1}] \times \bar{\Omega}, \\ \boldsymbol{X}(\boldsymbol{x}, t_{n+1}; t_{n+1}) &= \boldsymbol{x}. \end{aligned} \tag{9}$$

The existence and uniqueness of the solution of (9) for all times t are established, see for instance [18]. To obtain the departure points $\{\boldsymbol{X}_{hj}^n\}$ for each mesh point $\boldsymbol{x}_j$, $j = 1, \ldots, M$, we use the algorithm proposed in [29] which accurately solves (9) with a second-order accuracy. We write the solution of (9) in the form of

ICCS Camera Ready Version 2021
To cite this paper please use the final published version:
DOI: 10.1007/978-3-030-77980-1_17

$$\boldsymbol{X}_{hj}^{n} = \boldsymbol{x}_j - \boldsymbol{\alpha}_{hj}, \qquad j = 1, \ldots, M, \tag{10}$$

where the displacement $\boldsymbol{\alpha}_{hj}$ is calculated by the iterative procedure

$$\begin{aligned} \boldsymbol{\alpha}_{hj}^{(0)} &= \frac{\Delta t}{2}\Big(3\boldsymbol{u}_h^n\left(\boldsymbol{x}_j\right) - \boldsymbol{u}_h^{n-1}\left(\boldsymbol{x}_j\right)\Big), \\ \boldsymbol{\alpha}_{hj}^{(k+1)} &= \frac{\Delta t}{2}\left(3\boldsymbol{u}_h^n\left(\boldsymbol{x}_j - \frac{1}{2}d_{hj}^{(k)}\right) - \boldsymbol{u}_h^{n-1}\left(\boldsymbol{x}_j - \frac{1}{2}d_{hj}^{(k)}\right)\right), \qquad k = 0, 1, \ldots. \end{aligned} \tag{11}$$

To evaluate values of the approximate velocities in (11), we first identify the mesh element $\widehat{\mathcal{K}}_j$ where $\boldsymbol{x}_j - \dfrac{1}{2}\boldsymbol{\alpha}_{hj}^{(k)}$ resides. Then, a finite element interpolation on $\widehat{\mathcal{K}}_j$ is performed according to (2). Thus, assuming that the pairs $(\boldsymbol{X}_{hj}^n, \widehat{\mathcal{K}}_j)$ along with the mesh point values $\left\{\mathcal{T}_j^n\right\}$ are known for all $j = 1, \ldots, M$, we can approximate the values $\left\{\widehat{\mathcal{T}}_j^n\right\}$ by

$$\widehat{\mathcal{T}}_j^n := \Theta_h^n(\boldsymbol{X}_{hj}^n) = \sum_{k=1}^{M} \mathcal{T}_k \phi(\boldsymbol{X}_{hj}^n). \tag{12}$$

The solution $\left\{\widehat{\Theta}_h^n\right\}$ of the heat equation (1b) is then obtained by

$$\widehat{\Theta}_h^n(\boldsymbol{x}) = \sum_{j=1}^{M} \widehat{\mathcal{T}}_j^n \phi_j(\boldsymbol{x}). \tag{13}$$

Notice that (12) and (13) are respectively, the local and global approximations of the solutions Θ_h^n at the departure points $\boldsymbol{X}_{hj}^n$.

2.2 Time integration procedure

For time integration, we use a second-order semi-implicit Crank-Nicolson scheme. Then, we obtain the discretization of the Darcy-heat problem (5) as: Find $\left(\boldsymbol{u}_h^{n+1}, p_h^{n+1}, \Theta_h^{n+1}\right)$ in $\mathbf{S}_h \times Q_h \times R_h$ such that

$$\int_\Omega \nu(\widehat{\Theta}_h^n)\boldsymbol{u}_h^{n+1} \cdot \mathbf{s}_h \, d\Omega - \int_\Omega p_h^{n+1} \nabla \cdot \mathbf{s}_h \, d\Omega = \int_\Omega \boldsymbol{f}(\widehat{\Theta}_h^n) \cdot \mathbf{s}_h \, d\Omega, \quad \forall\, \mathbf{s}_h \in \mathbf{S}_h, \tag{14a}$$

$$\int_\Omega q_h \, \nabla \cdot \boldsymbol{u}_h^{n+1} \, d\Omega = \int_\Omega \left(p_h^{n+1} - \Pi_{k-1} p_h^{n+1}\right)\left(q_h - \Pi_{k-1} q_h\right) \, d\Omega, \qquad \forall\, q_h \in Q_h,$$

$$\int_\Omega \frac{\Theta_h^{n+1} - \widehat{\Theta}_h^n}{\Delta t} r_h \, d\Omega + \frac{\kappa}{2}\int_\Omega \nabla\Theta_h^{n+1} \cdot \nabla r_h \, d\Omega = \int_\Omega g_h^n r_h \, d\Omega + \frac{\kappa}{2}\int_\Omega \nabla\widehat{\Theta}_h^n \cdot \nabla r_h \, d\Omega, \qquad \forall\, r \in R_h, \tag{14b}$$

where $\widehat{\Theta}_h^n$ are the characteristics curves obtained by (13) and g_h^n the function given by

$$g_h^n = \frac{1}{\Delta t}\int_{t_n}^{t_{n+1}} g_h(s) \, ds.$$

For the existence and uniqueness of the solution of (14), we consider the following assumptions:

ICCS Camera Ready Version 2021
To cite this paper please use the final published version:
DOI: 10.1007/978-3-030-77980-1_17

ASSUMPTION **1** *The functions ν, $\boldsymbol{f}$ and g are assumed to verify:*

1. *ν is Lipschitz continuous and there exist two strictly positive constants ν_1 and ν_2 such that*
$$\nu_1 \leq \nu(\xi) \leq \nu_2, \qquad \forall\, \xi \in \mathbb{R}.$$
2. *$\boldsymbol{f}$ is Lipschitz with respect to its variable Θ, i.e.,*
$$\|\boldsymbol{f}(\Theta)\|_{L^\infty(0,T;L^2(\Omega)^d)} \leq c_{\boldsymbol{f}} \|\Theta\|_{L^\infty(0,T;L^2(\Omega)^d)},$$
where $c_{\boldsymbol{f}}$ is a positive constant.
3. $g \in L^2\left(0,T;L^2(\Omega)\right)$.

ASSUMPTION **2** *For all $p \in L^2(\Omega)$, the operator Π_{k-1} defined in (8) is assumed to satisfy :*

1. *Π_{k-1}: $L^2(\Omega) \longrightarrow L^2(\Omega)$ is continuous and*
$$\|\Pi_{k-1}p\|_{L^2(\Omega)} \leq c \|p\|_{L^2(\Omega)}, \tag{15}$$
where c is a positive constant independent of h.
2. *The properties of Π_{k-1} must be augmented by the approximation*
$$\|p - \Pi_{k-1}p\|_{L^2(\Omega)} \leq c' h\, |p|_{H^1(\Omega)}, \tag{16}$$
where c' is a positive constant independent of h.

Thus, for the a priori bounds for the numerical solutions, we have the following Theorem:

THEOREM **1** *At each time step t_n and for given $\widehat{\Theta}_h^n \in R_h$, problem (14) has a unique solution*
$(\boldsymbol{u}_h^{n+1}, p_h^{n+1}, \Theta_h^{n+1})$ in $\mathbf{S}_h \times Q_h \times R_h$ that verifies the following bounds:

$$\left\|\boldsymbol{u}_h^{n+1}\right\|_{L^2(\Omega)^d}^2 \leq \left(\frac{c_{\boldsymbol{f}}}{\nu_1}\right)^2 \left\|\widehat{\Theta}_h^n\right\|_{L^2(\Omega)^d}^2 + ch^2 \left|p_h^{n+1}\right|_{H^1(\Omega)}^2, \tag{17}$$

$$\left\|\Theta_h^{n+1}\right\|_{L^2(\Omega)} - \left\|\widehat{\Theta}_h^n\right\|_{L^2(\Omega)} \leq \Delta t \left\|g_h^n\right\|_{L^2(\Omega)}, \tag{18}$$

where c is a positive constant independent of h. □

PROOF. It is clear that the Darcy equations (7) have a unique solution since they satisfy the stabilized inf-sup condition [4,5]. Let a and b be two real numbers. For any positive real number ϵ, we have the well-known Young's inequality

$$ab \leq \frac{1}{2\epsilon}a^2 + \frac{1}{2}\epsilon b^2. \tag{19}$$

By testing equations (14a) with $\mathbf{s}_h = \boldsymbol{u}_h$ and $q_h = p_h$ and using the Cauchy-Schwarz inequality and (19) with $\epsilon = \dfrac{\nu_1}{c_{\boldsymbol{f}}}$, along with Assumptions 1 and 2, we immediately derive (17).

ICCS Camera Ready Version 2021
To cite this paper please use the final published version:
DOI: 10.1007/978-3-030-77980-1_17

Next, knowing $\boldsymbol{u}_h^n \in \mathbf{S}_h$ and thus $\widehat{\Theta}_h^n$, the heat equation (14b) admits also a unique solution $\Theta_h^{n+1} \in R_h$. Thus, if we take $r_h = \Theta_h^{n+1} + \widehat{\Theta}_h^n$ in (14b), we obtain and use the Cauchy-Schwarz and triangle inequalities, we easily get the inequality (18). ■

It is clear that the heat equation (14b) gives rise to the linear system form

$$\Big([\mathbf{M}] + \frac{\Delta t}{2}\,[\mathbf{S}]\Big)\boldsymbol{T}^{n+1} = [\mathbf{M}]\left(\widehat{\boldsymbol{T}}^n + \Delta t\,\boldsymbol{G}^n)\right) - \frac{\Delta t}{2}\,[\mathbf{S}]\,\widehat{\boldsymbol{T}}^n, \tag{20}$$

with $\boldsymbol{T}^{n+1} = \left(\mathcal{T}_1^{n+1}, \ldots, \mathcal{T}_M^{n+1}\right)^T$, $\widehat{\boldsymbol{T}}^n = \left(\widehat{\mathcal{T}}_1^n, \ldots, \widehat{\mathcal{T}}_M^n\right)^T$ and $\boldsymbol{G}^n = (g_1^n, \ldots, g_M^n)^T$ being the source term vector. Here, $[\mathbf{M}]$ and $[\mathbf{S}]$ are the mass and stiffness matrices whose elements are given respectively by

$$m_{ij} = \int_\Omega \phi_j \phi_i \, d\Omega, \qquad s_{ij} = \int_\Omega \nabla\phi_j \nabla\phi_i \, d\Omega, \qquad i,j = 1, \ldots, M.$$

Thus, the solution of the coupled Darcy-heat problem (1) can be reformulated in matrix form as

$$\begin{pmatrix} [\mathbf{A}] & [\mathbf{B}] & [\mathbf{O}] \\ [\mathbf{B}]^T & [\mathbf{D}] & [\mathbf{O}] \\ [\mathbf{O}] & [\mathbf{O}] & \left[\widehat{\mathbf{M}}\right] \end{pmatrix} \begin{pmatrix} \mathbb{U} \\ \mathbb{P} \\ \mathbb{T} \end{pmatrix} = \begin{pmatrix} \mathbb{F} \\ \mathbb{O} \\ \widehat{\mathbb{R}} \end{pmatrix}, \tag{21}$$

where $\mathbb{U}$, $\mathbb{P}$ and $\mathbb{T}$ are M-valued vectors with unknowns entries $\mathcal{U}_j^n$, $\mathcal{P}_j^n$ and $\mathcal{T}_j^n$ $(j = 1, \ldots, M)$, respectively, as defined in (2). In (21), $[\mathbf{O}]$ is the M square zero matrix, $[\mathbf{A}]$, $[\mathbf{B}]$ and $[\mathbf{D}]$ are square $M \times M$-valued matrices whose elements entries, according to (7), are respectively given by

$$a_{ij} = \int_\Omega \varphi_j \cdot \varphi_i \, d\Omega, \qquad b_{ij} = -\int_\Omega \phi_j (\nabla \cdot \varphi_i) \, d\Omega,$$
$$d_{ij} = \int_\Omega (\phi_j - \Pi_{k-1}\phi_j)\,(\phi_i - \Pi_{k-1}\phi_i)\;\, d\Omega,$$

where $i,j = 1, \ldots, M$, and $\left[\widehat{\mathbf{M}}\right]$ is the matrix given by $\left[\widehat{\mathbf{M}}\right] = [\mathbf{M}] + \frac{\Delta t}{2}\,[\mathbf{S}]$. In the right-hand side of (21), $\mathbb{F}$ is the M-valued vector with entries

$$F_j = \int_\Omega \boldsymbol{f}(\widehat{\mathcal{T}}_j^n) \cdot \varphi_i \, d\Omega, \qquad i,j = 1, \ldots, M,$$

$\mathbb{O}$ is the zero vector in $\mathbb{R}^M$ and $\widehat{\mathbb{R}}$ is the right-hand side of (20).

To summarize, the implementation of the proposed semi-Lagrangian unified element method for solving the coupled Darcy-heat equations (1) is carried out following the steps in Algorithm 1. Note that, since only the right-hand side of the linear system (21) changes at subsequent time steps, it is convenient to use a Cholesky factorization at the first time step thus the solution is reduced into subsequent forward and backward substitutions. This can significantly increase the efficiency when a large number of time steps is required, compared to updating the matrix and fully solving the system at every time step.

ICCS Camera Ready Version 2021
To cite this paper please use the final published version:
DOI: 10.1007/978-3-030-77980-1_17

Algorithm 1

1: Assemble and store the matrices associated to the linear system (21).
2: **while** $t_{n+1} \leq T$ **do**
3: **for** each mesh element $\mathcal{K}_j$ **do**
4: Calculate the departure point $\boldsymbol{X}_j^n$ using the algorithm (11).
5: Search-locate the mesh element $\widehat{\mathcal{K}}_j$ where $\boldsymbol{X}_j^n$ belongs.
6: Evaluate the solutions $\widehat{\Theta}_j^n = \Theta^n(\boldsymbol{X}_j^n)$ using (12).
7: **end for**
8: Assemble and store the right-hand sides associated to the linear system (21).
9: Compute the solution of (1) by solving the linear system (21).
10: **end while**

3 Numerical experiments

To validate the accuracy and performance of the proposed semi-Lagrangian finite element method, we present numerical results for two coupled Darcy-heat problems. All the computations are performed using unstructured triangular meshes with different element densities and by using the quadratic P_2 elements for all the solutions in the model (1). The obtained linear system of algebraic equations (21) is solved using the conjugate gradient solver with incomplete Cholesky decomposition. Moreover, all stopping criteria for iterative solvers are set to 10^{-7} which is small enough to guarantee that truncation errors in the algorithm dominate the total numerical errors.

3.1 Accuracy coupled Darcy-heat problem

In this test example, We consider the following time-dependent coupled Darcy-heat equations

$$\begin{aligned} \nu(\Theta)\boldsymbol{u} + \nabla p &= \big(\Theta + f(x,y,t)\big)\boldsymbol{j}, && (x,y,t) \in \Omega \times [0,T], \\ \nabla \cdot \boldsymbol{u} &= 0, && (x,y,t) \in \Omega \times [0,T], \\ \frac{\partial \Theta}{\partial t} + \boldsymbol{u} \cdot \nabla \Theta - \kappa \nabla^2 \Theta &= g(x,y,t), && (x,y,t) \in \Omega \times [0,T], \end{aligned} \tag{22}$$

supplemented with the following initial condition

$$\Theta(x,y,0) = 0 \qquad (x,y) \in \Omega. \tag{23}$$

In (22), $\boldsymbol{j} = (0,1)^\top$ is the unit vector in the upward direction, $\Omega = [0,3] \times [0,3]$, and $\nu(\Theta) = \Theta + 1$. The functions $f(x,y,t)$ and $g(x,y,t)$ are calculated such that the exact solution of (22) is given by

$$\boldsymbol{u}(x,y,t) = e^{-t/4} curl\psi, \qquad p(x,y,t) = (t+1)\cos(\frac{\pi}{3}x)\cos(\frac{\pi}{3}y),$$

$$\Theta(x,y,t) = \sin(t)x^2(x-3)^2y^2(y-3)^2,$$

ICCS Camera Ready Version 2021
To cite this paper please use the final published version:
DOI: 10.1007/978-3-030-77980-1_17

Table 1. Relative L^2-error and convergence rates obtained for the pressure, velocity and temperature solutions in the accuracy test example of the coupled Darcy-heat problem at time $t = 1$.

		Pressure p		Velocity u		Velocity v		Temperature Θ	
h	Iter	L^2-error	rate	L^2-error	rate	L^2-error	rate	L^2-error	rate
$\frac{1}{16}$	14.2	1.897561E-03	—	5.88932E-01	—	6.85811E-01	—	1.59171E-02	—
$\frac{1}{32}$	13.6	5.26369E-04	1.85	1.56710E-01	1.91	1.18123E-01	1.92	4.17711E-03	1.93
$\frac{1}{64}$	12.1	1.44001E-04	1.87	4.14113E-02	1.92	3.03099E-02	1.93	1.05886E-03	1.98
$\frac{1}{128}$	11.1	3.75290E-05	1.94	1.06439E-02	1.96	7.73669E-03	1.97	2.66556E-04	1.99
$\frac{1}{256}$	10.7	9.18917E-06	2.03	2.64259E-03	2.01	1.90754E-03	2.02	6.57216E-05	2.02

where the function ψ is defined as

$$\psi(x, y, t) = e^{-3\left((x-1)^2+(y-1)^2\right)}.$$

In our numerical simulations, the diffusion coefficient value is $\kappa = 5 \times 10^{-4}$ and the time step $\Delta t = 0.05$. Table 1 shows the averaged number of iterations in the linear solver, the relative L^2-errors and convergence rates at time $t = 1$ for the pressure p, the velocity $\boldsymbol{u} = (u, v)^\top$ and the temperature Θ using different structured meshes with uniform step h. It is obvious that, increasing the mesh density in the numerical simulations results in a decrease in the number of iterations needed for the linear solver and in the relative L^2-error for all variables and thus, a good approximation for the pressure, velocity and temperature solutions at the time in question. As expected, the proposed semi-Lagrangian finite element method converges at about the same rate for all meshes and for all solutions confirming a second-order accuracy.

3.2 Moving thermal front past an array of cylinders

In this second example, we consider a problem of moving thermal front in a channel past an array of circular cylinders. We present the numerical solution of the system of equations (1) in a channel of length $L = 4$ and height $H = 1$. The channel consists of 16 circular cylinders with equal diameter and uniformly distributed in the second quarter of the channel at the domain $[1, 2] \times [0, 1]$. In [3], a similar computational domain was considered but with square-shaped obstacles, and in order to study the incompressible Navier-Stokes equations. Here, no-slip boundary condition is imposed at all cylinder walls. The left and right vertical walls are respectively, at dimensionless temperatures $\Theta = 0.5$ and $\Theta = -0.5$ whereas, the top and bottom walls are insulated. Initially, the flow is at cold rest *i.e.*, $\boldsymbol{u} = \boldsymbol{0}$ and $\Theta = -0.5$. In our simulations, a non-linear viscosity defined by $\nu(\Theta) = \sin(\Theta) + 2$ is used in (1), the source terms $\boldsymbol{f} = \boldsymbol{0}$ and $g = 0$. In order to ensure accuracy and efficiency in the numerical method, we

ICCS Camera Ready Version 2021
To cite this paper please use the final published version:
DOI: 10.1007/978-3-030-77980-1_17

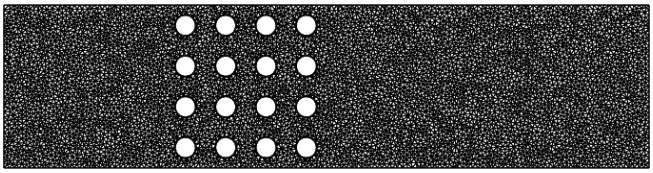

Fig. 1. Mesh used for the moving thermal front past an array of 16 cylinders of equal radius $R = 0.125$ uniformly distributed in a channel of length $L = 4$ and height $H = 1$. Here, the mesh contains 12224 triangular elements and 25295 nodes.

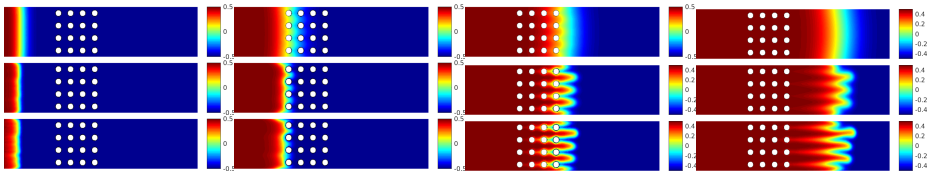

Fig. 2. Results for temperature for $\nu(\Theta) = \sin(\Theta) + 2$. From left to right: $t = 1$, $t = 3$, $t = 5$ and $t = 7$. From top to bottom: $\kappa = 0.01$, $\kappa = 0.001$, and $\kappa = 0.0005$.

use the unstructured triangular mesh depicted in Figure 1 with 12224 elements and 25295 nodes in our simulations. To approximate the temperature, velocity and pressure solutions, we use the quadratic P_2 finite elements. In Figure 2 and Figure 3, we display the results obtained for the temperature and velocity fields at four different instants namely, $t = 1$, $t = 3$, $t = 5$ and $t = 7$. To examine effects of diffusion in the moving thermal front past the cylinders, we present numerical results for three different values taken for the diffusion coefficient, $\kappa = 10^{-2}$, 10^{-3} and 5×10^{-4}. For a better insight, Figure 4 illustrates the vertical cross-sections at $x = 2.05$ of the temperature and the u-velocity at time $t = 5$ using the considered diffusion coefficient. It is clear that the cross-sections in Figure 4 show good symmetry in the numerical simulations. Similar features, not presented here, have been obtained at other locations in the channel using different values of κ. The results clearly illustrate the influence of the diffusion variation on both the temperature patterns and velocity fields.

Indeed, when the diffusion coefficient κ decreases, the transport speed increases with the size of the thermal front exhibiting steep gradients with different magnitudes, thin boundary layer, and separating shear layers. It is also worth noting that when the diffusion value is set to $\kappa = 5 \times 10^{-4}$, the flow becomes convection-dominated and steep fronts along with shock solutions appear in the temperature solution. For the considered Darcy-heat problem, these results obviously show that the small complex structures of the temperature being well captured by the proposed semi-Lagrangian finite element method. In fact, the computed solutions remain stable and highly accurate even when a relatively

ICCS Camera Ready Version 2021
To cite this paper please use the final published version:
DOI: 10.1007/978-3-030-77980-1_17

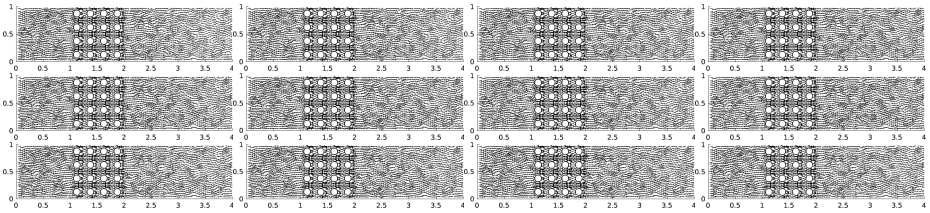

Fig. 3. Results for velocities for $\nu(\Theta) = \sin(\Theta) + 2$. From left to right: $t = 1$, $t = 3$, $t = 5$ and $t = 7$. From top to bottom: $\kappa = 0.01$, $\kappa = 0.001$, and $\kappa = 0.0005$.

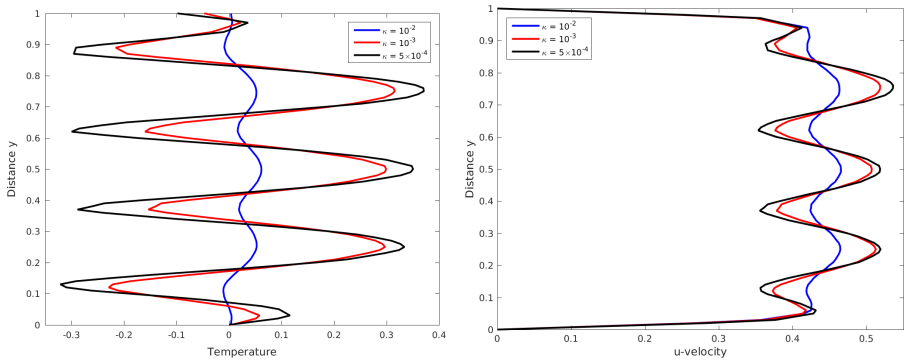

Fig. 4. Vertical cross-sections obtained in the channel at $x = 2.05$ for the temperature (left plot) and the u-velocity (right plot) for the Darcy-heat problem at time $t = 5$ using different diffusion coefficient values $\kappa = 10^{-2}, 10^{-3}$ and 5×10^{-4}.

coarse mesh is used, and the numerical resolution does not require the use of small time steps and mixed finite element discretizations.

4 Conclusions

In this study, we have presented a semi-Lagrangian finite element method for the numerical solution of time-dependent Darcy-heat problems. The governing equations consist of a nonlinear Darcy problem, with a variable viscosity, for the flow field and pressure coupled with a time-dependent convection-diffusion equation for the heat transfer. The enhanced method consists of coupling the semi-Lagrangian approach with a Galerkin finite element discretization on unstructured grids. To stabilize the solutions, we use a polynomial pressure-projection stabilization approach enabling the use of equal-order finite element approximations for all solutions in the coupled problem. The proposed method avoids mixed finite element formulations which generally require a higher computational cost for mesh generation and element matrix assembly. In our numerical

ICCS Camera Ready Version 2021
To cite this paper please use the final published version:
DOI: 10.1007/978-3-030-77980-1_17

simulations, we use the P_2-type polynomials to formulate the finite element solutions. However, the method can also be extended to the use of higher order polynomials based on a similar formulation. Numerical results have been presented for a test example with known exact solutions. The method has also been applied for solving a moving thermal front problem past an array of cylinders using different diffusion values. The presented results support our expectations for an accurate and stable behaviour for all transport regimes considered. Future work will concentrate on the extension of this method to Darcy-heat problems in three-dimensional domains using high-order finite element discretizations on unstructured meshes.

References

1. Y. Amanbek, G. Singh, G. Pencheva, and M.F. Wheeler. Error indicators for incompressible Darcy flow problems using enhanced velocity mixed finite element method. *Computer Methods in Applied Mechanics and Engineering*, 363:112884, 2020.
2. J. Bear. Hydraulics of groundwater. *Springer-Verlag, New York, NY, USA*, 1979.
3. J. Bernsdorf, F. Durst, and M. Schäfer. Comparison of cellular automata and finite volume techniques for simulation of incompressible flows in complex geometries. *Int. J. Numer. Meth. Fluids*, 29:251–264, 1999.
4. C.R. Bochev, P.B. Dohrmann. A computational study of stabilized, low-order C^0 finite element approximations of Darcy equations. *Computational Mechanics.*, 38:223–323, 2006.
5. P.B. Bochev, C.R. Dohrmann, and M.D. Gunzburger. Stabilization of low-order mixed finite elements for the Stokes equations. *SIAM Journal on Numerical Analysis*, 44(1):82–101, 2006.
6. J.M. Boland and R. A. Nicolaides. Stable and semistable low order finite elements for viscous flows. *SIAM J. Numer. Anal.*, 22:474–492, 1985.
7. F. Brezzi. On existence, uniqueness, and approximation of saddle-point problems arising from Lagrangian multipliers. *RAIRO Model. Math. Anal. Numer.*, 21: 129–151, 1974.
8. N. Chalhoub, P. Omnes, T. Sayah, and R. El-Zahlaniyeh. Full discretization of time dependent convection-diffusion-reaction equation coupled with the Darcy system. *Calcolo*, 57:4, 2019.
9. Z. Chen and R. Ewing. Mathematical analysis for reservoir models. *SIAM J. Math. Anal.*, pages 30, 431–453, 1999.
10. G. De Marsily. Quantitative hydrogeology. *Groundwater Hydrology for Engineers; Academic Press: New York, NY, USA*, 1986.
11. M. Dejam and H. Hassanzadeh. Diffusive leakage of brine from aquifers during CO_2 geological storage. *Advances in Water Resources*, 111:36–57, 2018.
12. T.F. Douglas, J. Russell. Numerical methods for convection dominated diffusion problems based on combining the method of characteristics with finite elements or finite differences. *SIAM J. Numer. Anal.*, 19:871–885, 1982.
13. M. El-Amrani and M. Seaid. Numerical simulation of natural and mixed convection flows by Galerkin-characteristic method. *Int. J. Numer. Meth. Fluids.*, 53(12):1819–1845, 2007.

ICCS Camera Ready Version 2021
To cite this paper please use the final published version:
DOI: 10.1007/978-3-030-77980-1_17

14. M. El-Amrani and M. Seaid. An L^2-projection for the Galerkin-characteristic solution of incompressible flows. *SIAM Journal on Scientific Computing*, 33(6):3110–3131, 2011.
15. Mofdi El-Amrani and Mohammed Seaid. A galerkin-characteristic method for large-eddy simulation of turbulent flow and heat transfer. *SIAM Journal on Scientific Computing*, 30(6):2734–2754, 2008.
16. Mofdi El-Amrani and Mohammed Seaïd. A finite element semi-lagrangian method with l2 interpolation. *International Journal for numerical methods in engineering*, 90(12):1485–1507, 2012.
17. X. Feng. On existence and uniqueness results for a coupled system modeling miscible displacement in porous media. *J. Math. Anal. Appl.*, pages 194, 883–910, 1995.
18. C. Foicas, C. Guillopé, and R. R. Temam. Lagrangian representation of the flow. *J. Diff. Eqns*, 57:440–449, 1985.
19. M. Gunzburger. Finite element methods for viscous incompressible flows. *Academic Press, Boston*, 1989.
20. A. Halassi, J. Joundy, L. Salhi, and A. Taik. A meshfree method for heat explosion problems with natural convection in inclined porous media. *MATEC Web of Conferences*, 241, 01019, 2018.
21. A.-R.A. Khaled and K. Vafai. The role of porous media in modeling flow and heat transfer in biological tissues. *International Journal of Heat and Mass Transfer*, 46(26):4989–5003, 2003.
22. D. A. Nield and A. Bejan. *Convection in porous media*. Springer-Verlag, New York, second edition, 1999.
23. H. Notsu, H. Rui, and M. Tabata. Development and L2-analysis of a single-step characteristics finite difference scheme of second order in time for convection-diffusion problems. *J. Algorithms Comput. Technol.*, 7:343–380, 2013.
24. O. Pironneau. On the transport-diffusion algorithm and its applications to the Navier-Stokes equations. *Numer. Math.*, 38:309–332, 1982.
25. H. Rui and J. Zhang. A stabilized mixed finite element method for coupled Stokes and Darcy flows with transport. *Computer Methods in Applied Mechanics and Engineering*, 315:169–189, 2017.
26. L. Salhi, M. El-Amrani, and M. Seaid. A Galerkin-characteristic unified finite element method for moving thermal fronts in porous media. *Journal of Computational and Applied Mathematics*, page 113159, 2020.
27. L. Salhi, M. El-Amrani, and M. Seaid. A stabilized semi-Lagrangian finite element method for natural convection in Darcy flows. *Computational and Mathematical Methods*, page e1140, 2021.
28. M. Seaid. Semi-Lagrangian integration schemes for viscous flows. *Comp. Methods in App. Math.*, 4:392–409, 2002.
29. A. Temperton, C. Staniforth. An efficient two-time-level semi-Lagrangian semi-implicit integration scheme. *Quart. J. Roy. Meteor. Soc.*, 113:1025–1039, 1987.
30. Y. M. Xuan and W. Roetzel. Bioheat equation of the human thermal system. *Chemical Engineering Technology*, 20(4):268–276, 1997.

ICCS Camera Ready Version 2021
To cite this paper please use the final published version:
DOI: 10.1007/978-3-030-77980-1_17